Supporting Information

Nanochannels as Molecular Check Valves

Qian Yang‡, Xingyu Lin‡, Yafeng Wang, Bin Su*

Institute of Analytical Chemistry, Department of Chemistry, Zhejiang University, Hangzhou, 310058, China
E-mail: subin@zju.edu.cn

‡ These authors contributed equally to this work.

Table of Content

S1. TEM and SEM images of SNM and PDMS-SNM

Transmission electron microscopy (TEM) images were performed on a HT7700 microscope (Hitachi, Japan) operated at 120 kV. High-resolution scanning electron microscopy (SEM) was obtained on a SU8010 field-emission scanning electron microscope (Hitachi, Japan) without sputtering Pt. Cross-sectional TEM images of SNM were prepared by mechanically scraping small pieces of SNM from ITO glass, dispersion in ethanol and then deposition on carbon-coated copper grids. Top-view TEM images were measured for SNM and PDMS-SNM under the support of a 3 mm-in-diameter porous SiN grid, which was directly positioned on the TEM sample holder.

Fig. S1a and **S1b** show the cross-section view of TEM and SEM images of SNM, which show the SNM has a uniform thickness of ~60 nm and consists of vertically aligned nanochannels parallel to each other with a uniform channel size of 2 ~ 3 nm in diameter. **Fig. S1c** displays the top-view TEM image of the SNM, showing highly ordered pores with uniform pore size of 2 ~ 3 nm (bright spots). In addition, these pores orderly distribute over a big domain with a high density (4×10^{12} cm^{-2}, corresponding to relative pore density of 16.7%). After PDMS deposition, the morphology of PDMS/SNM was still unchanged as shown in **Fig. S1d**. However, the image turns a little fuzzy due to the presence of an ultrathin nonconductive PDMS layer on the top surface.

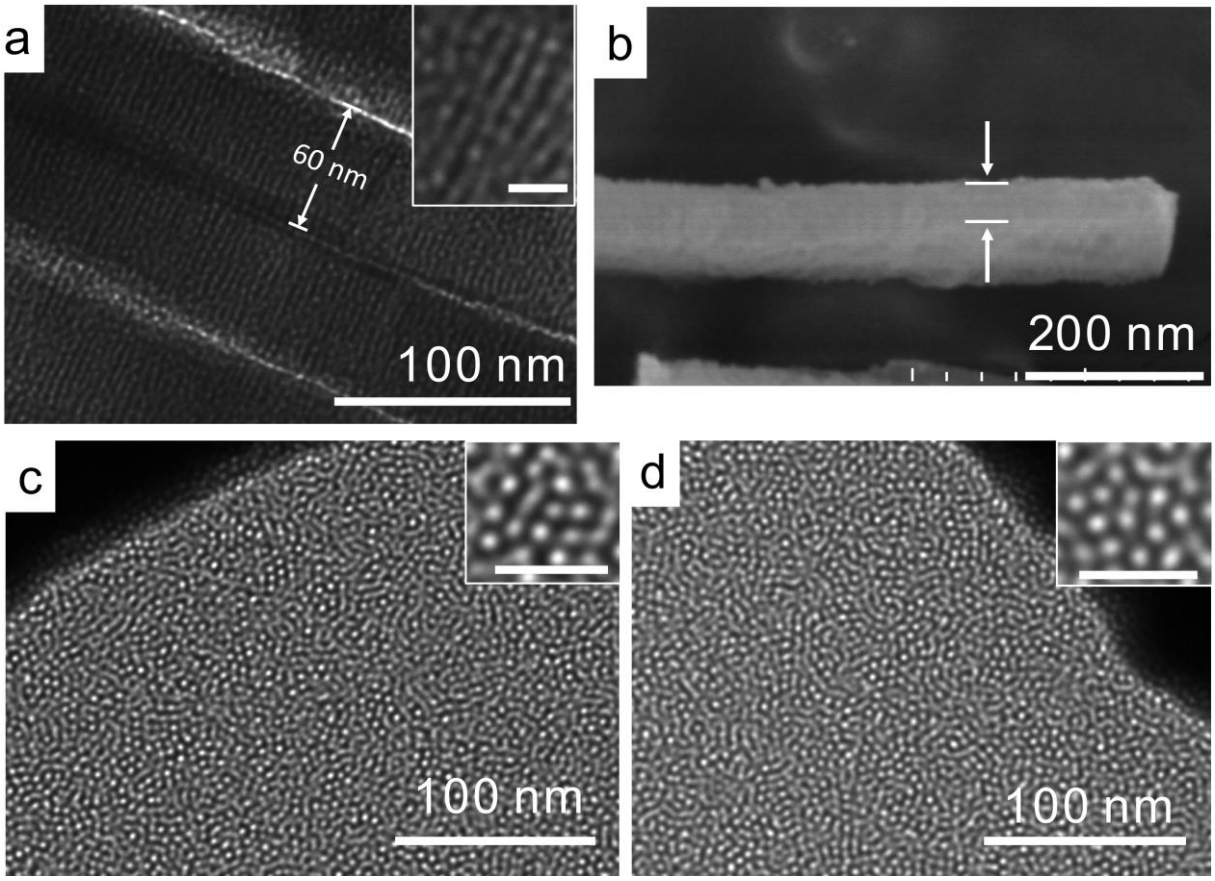

Fig. S1 (a) The cross-sectional view of TEM image of SNM. (b) The cross-sectional SEM image of SNM. (c, d) The top-view of TEM images of SNM (c) and PDMS-SNM (d). All the insets show the magnified images, and the scale bars are all 20 nm.

S2. Schematic diagram of the experimental setup for modifying PDMS

The SNM was positioned under a cured PDMS monolith supported by two pieces of glass slides, see below **Fig. S2**. The distance between the PDMS monolith and the SNM was about 1 mm. All these elements were put on the hot plate heated at 100 ^{o}C for 10 h to deposit PDMS oligomers on the surface of the SNM. The control experiment was investigated by heating the SNM at 100 ^{o}C for 10 h without PDMS monolith.

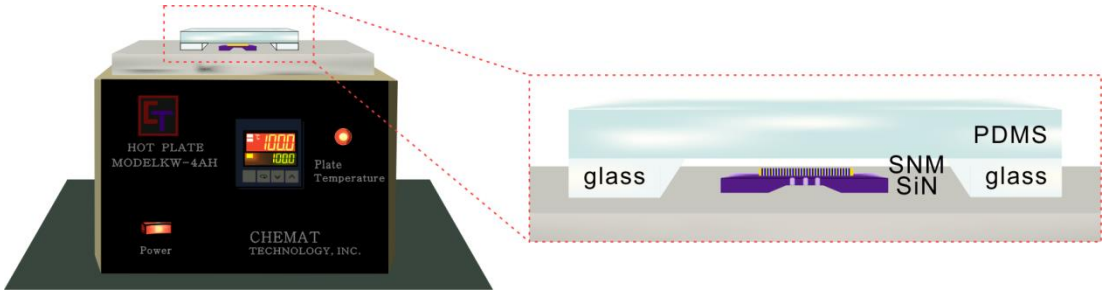

Fig. S2 Schematic illustration of asymmetric modification of the SNM on one side with PDMS. The size of stuff in the picture is not proportional to that of reality.

S3. Optimization of the working electrode and calibration curves with CVs

Electrochemical detection of low concentration of probes is usually difficult, especially at a low ionic strength (a low supporting electrolyte concentration). Here, we used a three-electrode configuration. An Ag/AgCl (saturated KCl) and a Pt wire were used as the reference electrode and the counter electrode, respectively. We first tried to use different commercial disk electrodes as the working electrode, including Au electrode, glass carbon electrode, Pt electrode, and ultramicroelectrode (Pt, radius = 25 μm), to detect 10 μM $Ru(NH_3)_6Cl_3$ in 1 mM KCl solution, as shown in **Fig. S3a** – 3**d**. No obvious redox peak current was observed with $Ru(NH_3)_6Cl_3$ in CVs, indicating that all of them are not suitable for detection in the present system. However, the ITO electrode displayed a distinct reduction peak current (see **Fig. S3e**). The results demonstrated that the ITO electrode was the optimal working electrode. The calibration curves of $Ru(NH_3)_6Cl_3$ and $K_3Fe(CN)_6$ in 1 mM KCl and 1 M KCl obtained with the ITO electrodes were shown in **Fig. S4**.

The absolute value of the slope of $Ru(NH_3)_6Cl_3$ in 1 mM KCl was 0.044 μA/μM. The standard deviation (SD) of the ITO electrodes under this condition was 0.0027. Therefore, the limit of detection (LOD) for $Ru(NH_3)_6Cl_3$ in 1 mM KCl solution was 0.18 μM, as calculated by **Eq. S1**.

$$\mathrm{LOD} = \frac{3\mathrm{SD}}{\mathrm{slope}} \qquad \text{(S1)}$$

.

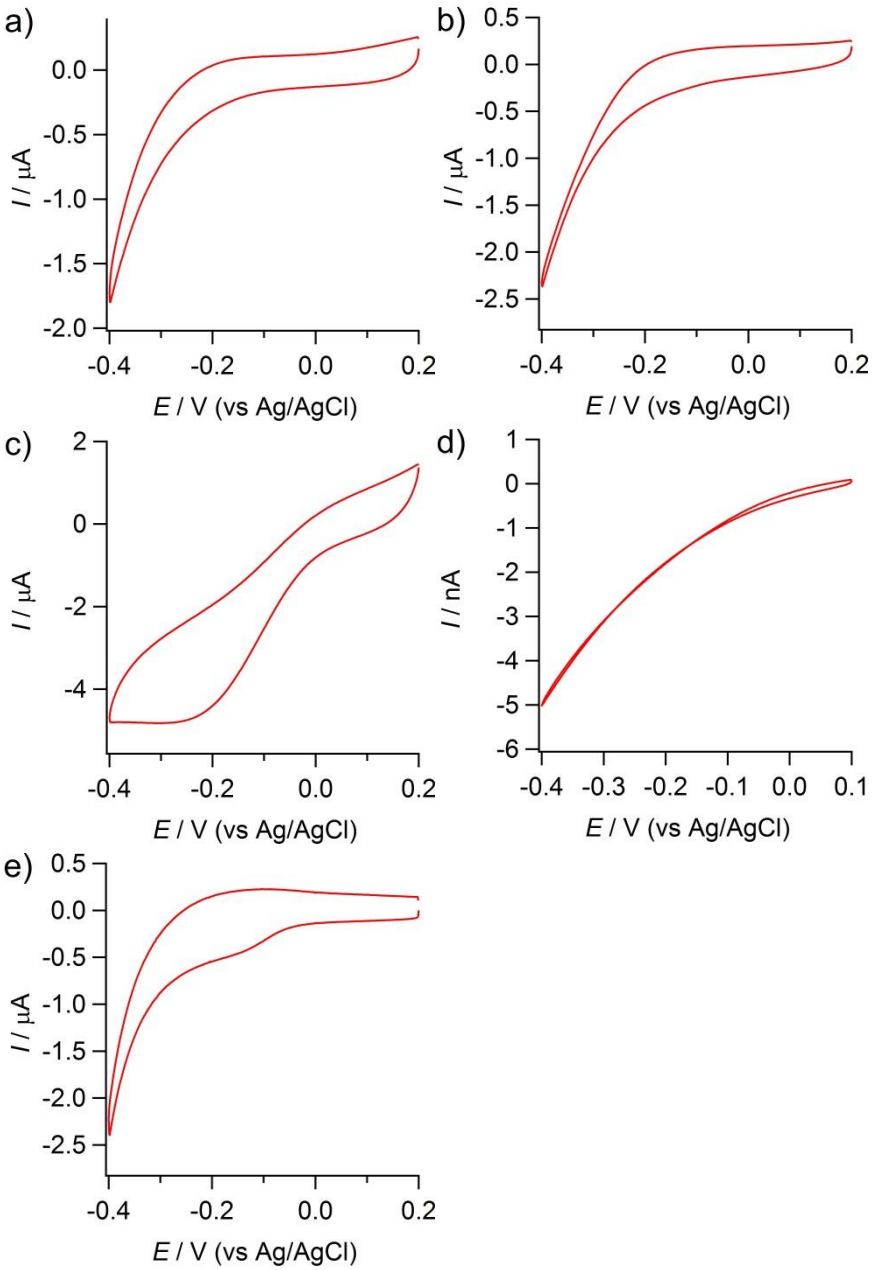

Fig. S3 CVs of 10 μM $Ru(NH_3)_6Cl_3$ in 1 mM KCl solution obtained with different working electrodes: (a) Au electrode, (b) glass carbon electrode, (c) Pt electrode, (d) Pt ultramicroelectrode, (e) ITO electrode. A Pt wire and an Ag/AgCl (saturated KCl) were used as the counter and the reference electrodes, respectively.

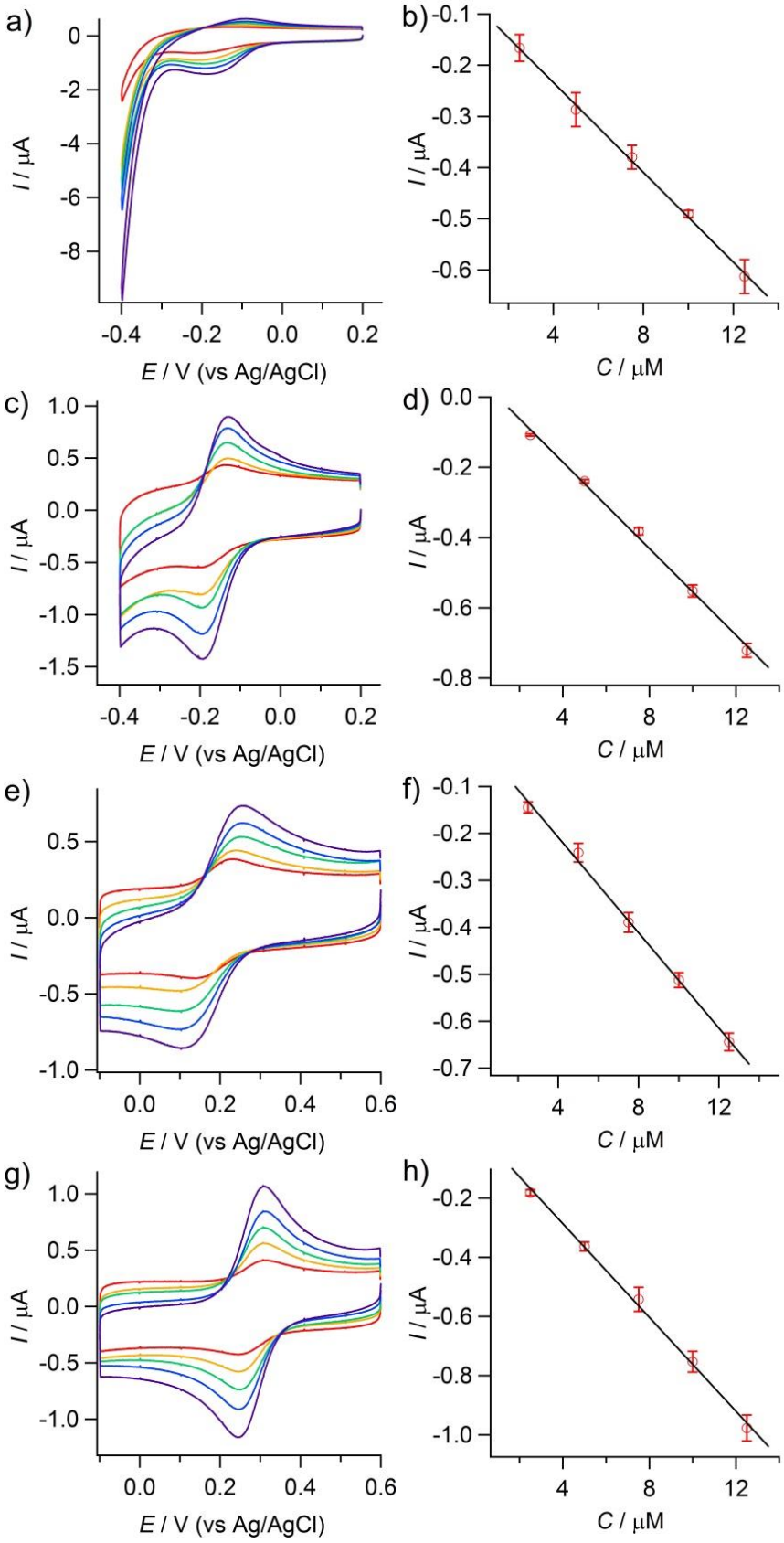

Fig. S4 (a, c) CVs and (b, d) calibration curves of $Ru(NH_3)_6Cl_3$ in 1 mM KCl (a, b) and 1 M KCl (c, d). (e, g) CVs and (f, h) calibration curves of $K_3Fe(CN)_6$ in 1 mM KCl (e, f) and 1 M KCl (g, h).

S4. Comparison of CVs of $Ru(NH_3)_6Cl_3$ in 1 mM KCl from different directions

Fig. S5 shows the CVs of $Ru(NH_3)_6Cl_3$ detected in the permeate solution after 60 h of free diffusion transport. If the feed solution was added to the SNM side, no obvious reduction current due to the reduction of $Ru(NH_3)_6Cl_3$ was observed (see the black curve in **Fig. S5**). If it was added to the PDMS side, an obvious reductive current peak was obtained (see the red curve in **Fig. S5**). It suggests that the PDMS-SNM can function as a molecular check valve, allowing the unidirectional transport of cationic $Ru(NH_3)_6^{3+}$.

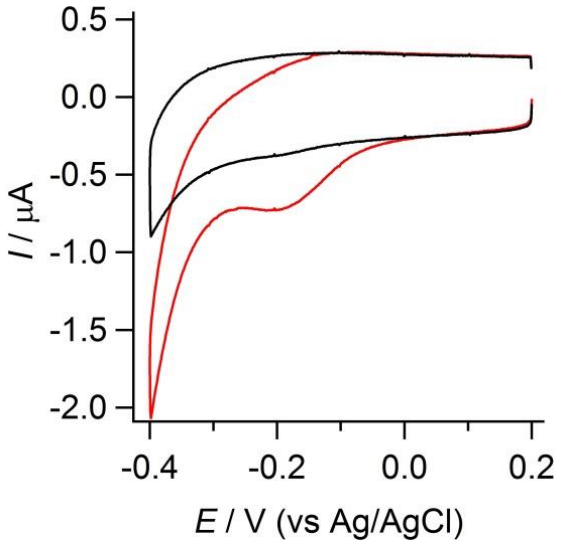

Fig. S5 CVs of $Ru(NH_3)_6Cl_3$ in the permeate solution after diffusion for 60 h. Both the feed and permeate solutions contained 1 mM KCl. The red line represents the probe transport through the membrane from the PDMS side ($C_{PDMS} > C_{SNM}$) and the black line represents that from the naked SNM side ($C_{SNM} > C_{PDMS}$).

S5. CVs of $Ru(NH_3)_6Cl_3$ diffusion from PDMS side to SNM side with different ionic strength of KCl

To quantitively investigate the relationship between the electrostatic interaction and hydrophobic force, the influence of other ionic strength of KCl was conducted when the $Ru(NH_3)_6Cl_3$ was added into the PDMS side initially. No obviouse redox current peak was shown in **Fig. S6** after 60 h, when the concentration of KCl was decreased to 0.1 M or 0.01 M. Integrate of the result in **Fig. 3b**, the diffusion of $Ru(NH_3)_6Cl_3$ was occurred from PDMS side to SNM side as long as the concentration of KCl smaller than 0.01 M, which meant the electrostatic interaction would play an important role when the concentration of KCl decreased to 1 mM.

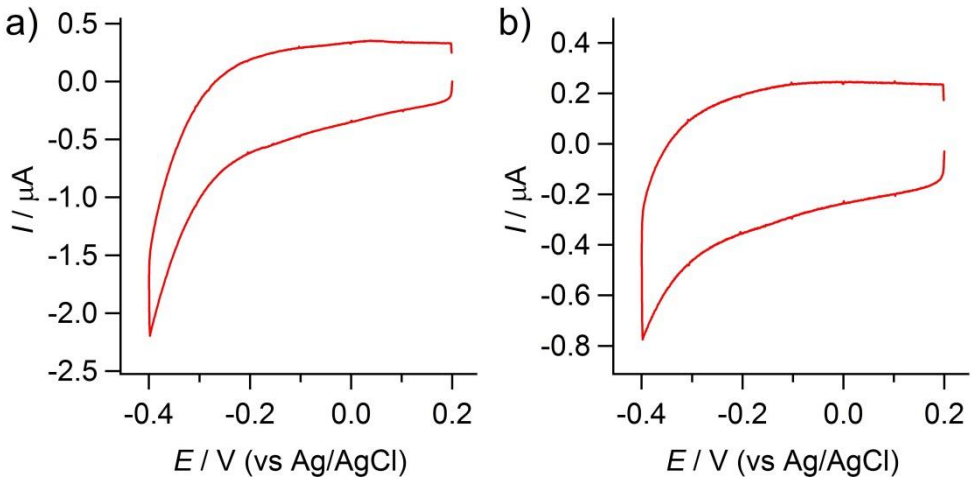

Fig. S6 CVs of $Ru(NH_3)_6Cl_3$ diffusion from PDMS side to SNM side in 0.1 M KCl (a) and 0.01 M KCl (b) after 60 h, respectively.

S6. Kinetic plots of $Ru(NH_3)_6Cl_3$ diffusion across the PDMS-SNM in 1 mM HCl

In order to clarify the importance of electrostatic interaction, similar experiments were also performed with 1mM HCl solution (pH = 3, low ionic strength), where nearly no electrostatic interaction existed because the isoelectric point of SNM was 3 ~ 4.[1] As shown in **Fig. S7a**, no $Ru(NH_3)_6Cl_3$ could be detected in the permeate cell from either side of the PDMS-SNM in this condition. This result demonstrates that the electrostatic interaction plays an important role in the unidirectional diffusion. Without the driving of electrostatic attraction, the positively charged molecules cannot pass the hydrophobic barrier, as discussed in the manuscript (see also **Fig. S7b**).

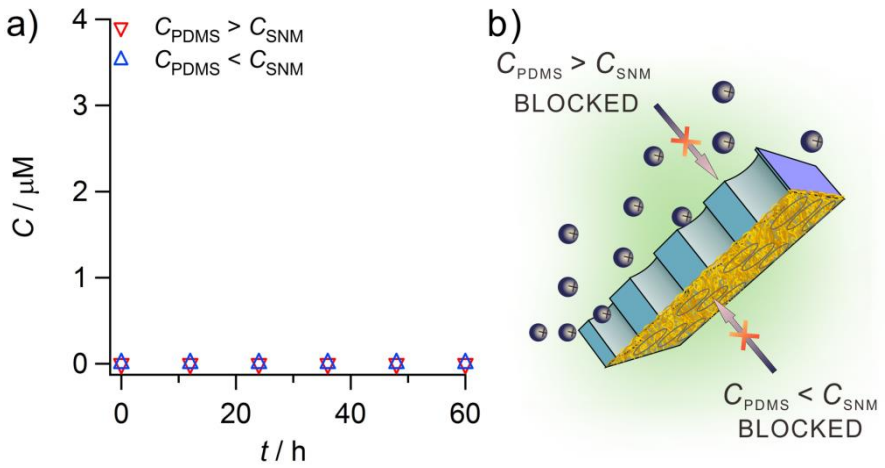

Fig. S7 (a) The kinetic plots of 5 mM $Ru(NH_3)_6Cl_3$ diffusion across the PDMS-SNM from either side in 1 mM HCl. (b) Schematic illustration of $Ru(NH_3)_6Cl_3$ diffusion through the PDMS-SNM membrane in 1 mM HCl.

S7. Kinetic plots of $Ru(NH_3)_6Cl_3$ diffusion across the PDMS-SNM-PDMS

Both sides of SNM were modified with PDMS by the method mentioned above. Briefly, after one side of SNM was modified with PDMS, the PDMS-SNM was reversed and the same modification process was performed on the other side for the other 10 h. The obtained nanochannel membrane was designated as PDMS-SNM-PDMS (**Fig. S8a**). As shown in **Fig. S8b**, the $Ru(NH_3)_6Cl_3$ could not be detected in the permeate solution even after 60 h from either side of the PDMS-SNM-PDMS. We suppose that although the $Ru(NH_3)_6Cl_3$ could diffuse the first layer of the PDMS as discussed in the manuscript, there was no electrostatic interaction outside of the second PDMS-layer so that the probe molecules were trapped and could not diffuse through the membrane.

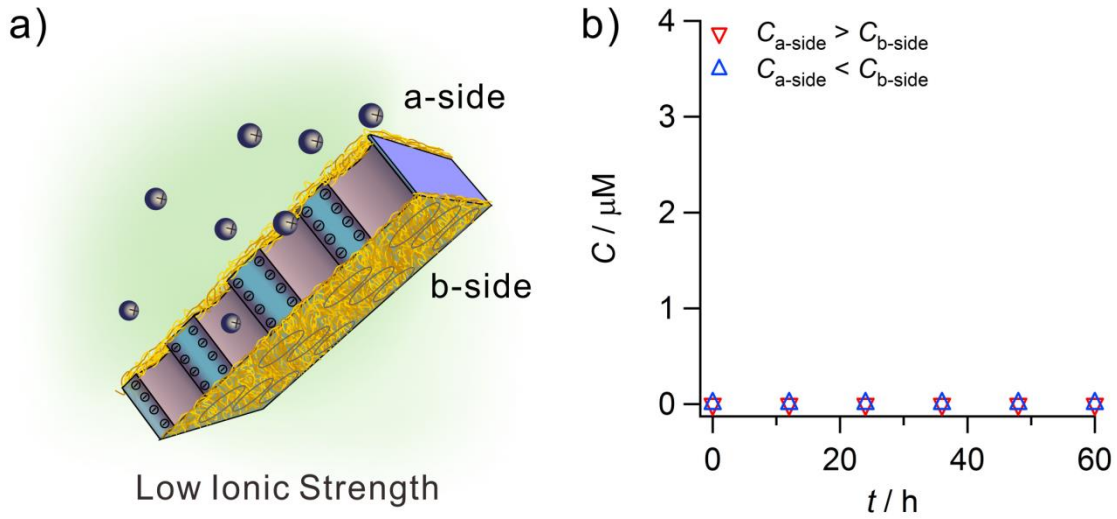

Fig. S8 (a) Schematic illustration of PDMS-SNM-PDMS membrane. And the two PDMS-layers were designated as a-side and b-side, respectively. (b) The kinetic plots of 5 mM $Ru(NH_3)_6Cl_3$ diffusion across the PDMS-SNM-PDMS membrane in the situation of 1 mM KCl.

S8. The numerical calculation of the thickness of electrical double layer (EDL) in nanochannels

The radial potential distribution in a nanochannel can be expressed by the Poisson-Boltzmann equation in cylindrical coordinates. And the formula is displayed in **Eq. S2** since the electrolyte was KCl using in this work.

$$\frac{\mathrm{d}^2\phi}{\mathrm{d}r^2}+\frac{1}{r}\frac{\mathrm{d}\phi}{\mathrm{d}r}=\frac{2n^0e}{\varepsilon}\sinh\left(\frac{e\phi}{kT}\right) \qquad \text{(S2)}$$

where ϕ is the potential at the distance r from the axis, and e, ε, k, T and n^0 are the electron charge, dielectric constant, Boltzmann constant, temperature and the number concentration of KCl, respectively.

Inside silica nanochannels, silanol groups can behave as weak acids with a pK_a of 6.77 (silanols are very weak bases, since the pK_a of $SiOH^+$ is –2.77).[2] Therefore, the surface charge density (σ_0) can be formulated by the **Eq. S3**,[3, 4]

$$\sigma_0=-\mathrm{F}\Gamma_\mathrm{t}\frac{10^{-\mathrm{pK_a}}}{\left[\mathrm{H^+}\right]_\mathrm{s}+10^{-\mathrm{pK_a}}} \qquad \text{(S3)}$$

where F is the Faraday constant, Γ_t is the total number site density of SiOH groups inside the nanochannels (4.6 OH/nm^2), and $\left[\mathrm{H^+}\right]_\mathrm{s}$ is the molar concentration of H^+ ions at the dielectric layer/liquid interface, which is $\left[\mathrm{H^+}\right]_\mathrm{s}=10^{-\mathrm{pH}}\exp\left(-\frac{F\phi_0}{RT}\right)$.

In the present system, the pH of KCl solution was 6.7 that was close to the pK_a of SiOH, thus resulting in an equivalent concentration of SiO^- and SiOH. Hence, ϕ_0 = 4.14 mV, which was much smaller than 25.67 mV. Therefore, **Eq. S2** can be simplified to **Eq. S4**.

$$\frac{\mathrm{d}^2\phi}{\mathrm{d}r^2}+\frac{1}{r}\frac{\mathrm{d}\phi}{\mathrm{d}r}=\kappa^2\phi \qquad \text{(S4)}$$

where $\kappa = \sqrt{\frac{2n^0 e^2}{\varepsilon kT}}$. Using the boundary conditions of $\phi = \phi_0$ at r = a and ϕ is finite at $r = 0$, **Eq. S4** can be integrated to obtain the potential distribution,

$$\phi(r) = \phi_0 \frac{I_0(\kappa r)}{I_0(\kappa a)} \qquad \text{(S5)}$$

where I_0 is the zero-order modified Bessel function of the first kind. And the numerical solution is shown in **Fig. S9**, where $a = 1.15$ nm and ϕ_0 = 4.14 mV are assigned.

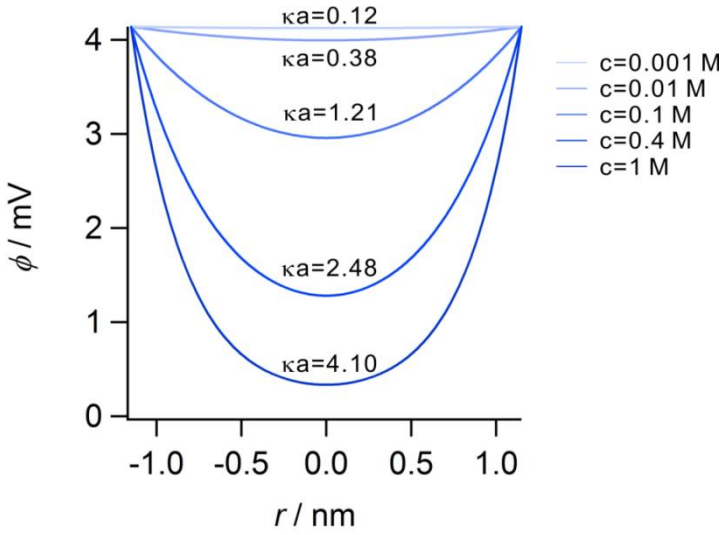

Fig. S9 The numerical solutions of Poisson-Boltzmann equation in nanochannels with 1.15 nm pore radius. The KCl concentrations from top to bottom are 0.001 M, 0.01 M, 0.1 M, 0.4 M, 1 M, respectively.

S9. Mechanism of the transport of anions across the PDMS-SNM

As shown in **Fig. S10**, $Fe(CN)_6^{3-}$ was unable to diffuse across the PDMS-SNM no matter in low or high ionic strength solutions. Because both electrostatic and hydrophobic forces repel its transport across the PDMS-SNM.

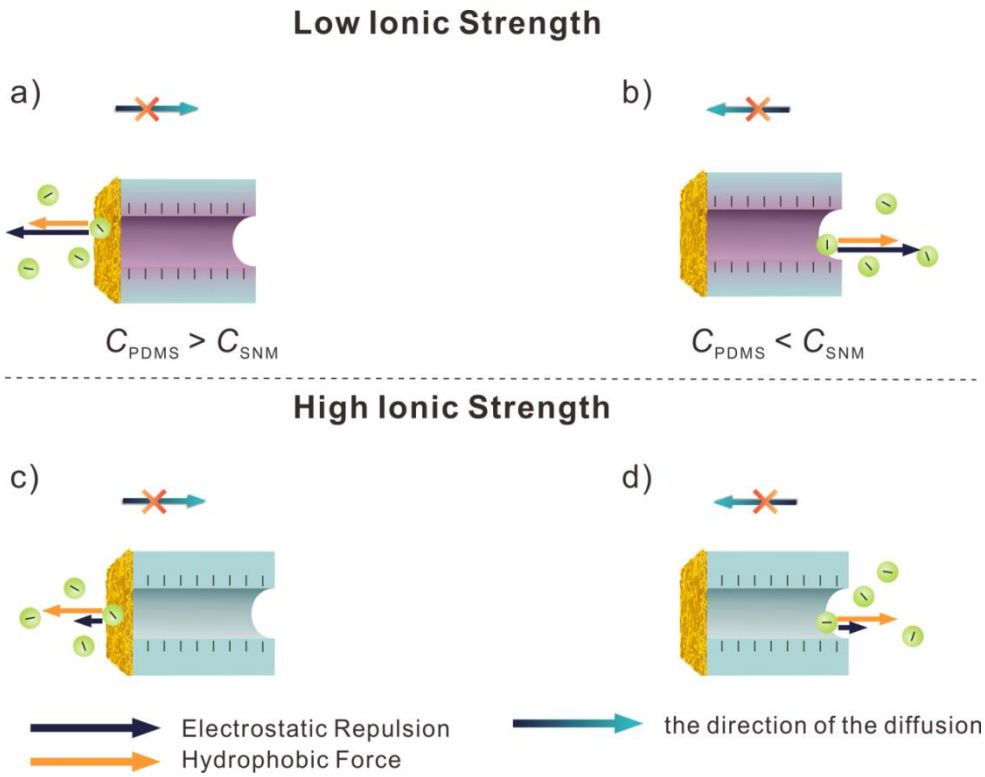

Fig. S10 Mechanism of anion transport through the PDMS-SNM at a low (a, b) and high (c, d) ionic strength. The anions are subject to both hydrophobic rejection and electrostatic repulsion, so the transport of anions is inhibited. The length of arrows schematically represents the magnitude of force.

References

1. X. Lin, Q. Yang, L. Ding and B. Su, *ACS Nano*, 2015, **9**, 11266–11277.
2. M. Tagliazucchi and I. Szleifer, *Chemically Modified Nanopores and Nanochannels*, Elsevier, 2016.
3. C. Hughes, L.-H. Yeh and S. Qian, *J. Phys. Chem. C*, 2013, **117**, 9322-9331.
4. M.-J. Huang, L. Mei, L.-H. Yeh and S. Qian, *Electrochem. Commun.*, 2015, **55**, 60-63.